



Locating and Quantifying Broadband Fan Sources Using In-Duct Microphones

Robert P. Dougherty
OptiNav, Inc., Redmond, Washington

Bruce E. Walker
Channel Islands Acoustics, Camarillo, California

Daniel L. Sutliff
Glenn Research Center, Cleveland, Ohio

NASA STI Program . . . in Profile

Since its founding, NASA has been dedicated to the advancement of aeronautics and space science. The NASA Scientific and Technical Information (STI) program plays a key part in helping NASA maintain this important role.

The NASA STI Program operates under the auspices of the Agency Chief Information Officer. It collects, organizes, provides for archiving, and disseminates NASA's STI. The NASA STI program provides access to the NASA Aeronautics and Space Database and its public interface, the NASA Technical Reports Server, thus providing one of the largest collections of aeronautical and space science STI in the world. Results are published in both non-NASA channels and by NASA in the NASA STI Report Series, which includes the following report types:

- **TECHNICAL PUBLICATION.** Reports of completed research or a major significant phase of research that present the results of NASA programs and include extensive data or theoretical analysis. Includes compilations of significant scientific and technical data and information deemed to be of continuing reference value. NASA counterpart of peer-reviewed formal professional papers but has less stringent limitations on manuscript length and extent of graphic presentations.
- **TECHNICAL MEMORANDUM.** Scientific and technical findings that are preliminary or of specialized interest, e.g., quick release reports, working papers, and bibliographies that contain minimal annotation. Does not contain extensive analysis.
- **CONTRACTOR REPORT.** Scientific and technical findings by NASA-sponsored contractors and grantees.

- **CONFERENCE PUBLICATION.** Collected papers from scientific and technical conferences, symposia, seminars, or other meetings sponsored or cosponsored by NASA.
- **SPECIAL PUBLICATION.** Scientific, technical, or historical information from NASA programs, projects, and missions, often concerned with subjects having substantial public interest.
- **TECHNICAL TRANSLATION.** English-language translations of foreign scientific and technical material pertinent to NASA's mission.

Specialized services also include creating custom thesauri, building customized databases, organizing and publishing research results.

For more information about the NASA STI program, see the following:

- Access the NASA STI program home page at <http://www.sti.nasa.gov>
- E-mail your question via the Internet to help@sti.nasa.gov
- Fax your question to the NASA STI Help Desk at 443-757-5803
- Telephone the NASA STI Help Desk at 443-757-5802
- Write to:
NASA Center for AeroSpace Information (CASI)
7115 Standard Drive
Hanover, MD 21076-1320



Locating and Quantifying Broadband Fan Sources Using In-Duct Microphones

Robert P. Dougherty
OptiNav, Inc., Redmond, Washington

Bruce E. Walker
Channel Islands Acoustics, Camarillo, California

Daniel L. Sutliff
Glenn Research Center, Cleveland, Ohio

Prepared for the
16th Aeroacoustics Conference
cosponsored by the American Institute of Aeronautics and Astronautics
and the Confederation of European Aerospace Societies
Stockholm, Sweden, June 7–9, 2010

National Aeronautics and
Space Administration

Glenn Research Center
Cleveland, Ohio 44135

Acknowledgments

This work was supported by the NASA NRA Contract NNC07CB02C “Improved Phased Array Techniques to Account for Extended Sources of Fan and Jet Noise.”

This work was sponsored by the Fundamental Aeronautics Program
at the NASA Glenn Research Center.

Level of Review: This material has been technically reviewed by technical management.

Available from

NASA Center for Aerospace Information
7115 Standard Drive
Hanover, MD 21076-1320

National Technical Information Service
5301 Shawnee Road
Alexandria, VA 22312

Available electronically at <http://gltrs.grc.nasa.gov>

Locating and Quantifying Broadband Fan Sources Using In-Duct Microphones

Robert P. Dougherty
OptiNav, Inc.
Redmond, Washington 98052

Bruce E. Walker
Channel Islands Acoustics
Camarillo, California 93010

Daniel L. Sutliff
National Aeronautics and Space Administration
Glenn Research Center
Cleveland, Ohio 44135

Abstract

In-duct beamforming techniques have been developed for locating broadband noise sources on a low-speed fan and quantifying the acoustic power in the inlet and aft fan ducts. The NASA Glenn Research Center's Advanced Noise Control Fan was used as a test bed. Several of the blades were modified to provide a broadband source to evaluate the efficacy of the in-duct beamforming technique. Phased arrays consisting of rings and line arrays of microphones were employed. For the imaging, the data were mathematically resampled in the frame of reference of the rotating fan. For both the imaging and power measurement steps, array steering vectors were computed using annular duct modal expansions, selected subsets of the cross spectral matrix elements were used, and the DAMAS and CLEAN-SC deconvolution algorithms were applied.

Introduction

Significant reduction in aircraft noise is required to meet ongoing noise regulation in the USA and Europe. Since the turbofan engine is a large contributor to aircraft noise, any overall reduction in aircraft noise must include engine noise reduction. In order to efficiently achieve noise reduction, detailed understanding of the physics of noise source generation is required. The NASA focus area—Fundamental Aeronautics, Subsonic: Fixed Wing Program—emphasizes developing technologies for diagnostics of noise for subsonic aircraft. The work described here is intended to advance the state of the art for imaging broadband fan noise of turbofan engines using microphones that are flush mounted in the outer wall of the bypass flow path of the nacelle. The recordings are post-processed to form images of broadband noise sources on the rotating blades and to measure the modal amplitudes and the sound power in the inlet and aft fan ducts. The blade acoustic images and mode maps are intended to help clarify the mechanism for fan broadband noise generation and to identify any problem areas on a given set of blades. The sound power measurement may be a convenient and more-precise substitute for far field microphones.

Nomenclature

\vec{x}_i	a microphone location
\vec{x}	a source point
μ, ν	microphone indices
S	a set of array microphone pairs, (μ, ν)
b	beamforming result
C	cross spectral matrix
\bar{C}	trimmed cross spectral matrix
w	beamforming weight vector
g	steering vector
PSF	array point spread function
J_m, Y_m	Bessel functions
φ_{mn}	mode function
m	spinning order
n	radial order

Array Configuration and Approaches

The NASA Glenn Research Center Aero-Acoustic Propulsion Laboratory is shown in Figure 1, and the Advanced Noise Control Fan rig (ANCF) therein is shown in Figure 2. The ANCF has an electrically driven fan, which, for this test, consisted of 16 blades. Four fan exit guide vanes, the minimum number allowed for vibration considerations, were installed. Arc arrays of external microphones, as shown in Figure 2, were used to determine the integrated sound power level in the inlet and aft sectors. Since no acoustic lining was installed, it is assumed that forward-propagating sound power in the inlet duct should equal the sound power derived from the forward-arc external array, and similarly for the sound power in the aft duct and the rear external microphones.



Figure 1.—Aero-Acoustic Propulsion Laboratory.

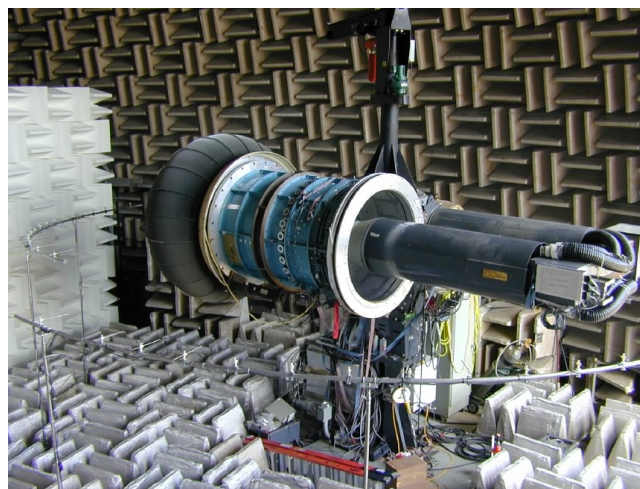


Figure 2.—Advanced Noise Control Fan.

Internal Microphone Arrays

The microphones used for the internal measurements are shown in Figures 3 to 6. Six sub-arrays of wall microphones: four rings of 30 microphones each labeled A, B, C, and E, a forward axial array of 16 microphones, and an aft axial array of 14 sensors are used for the current analysis. An additional 30-microphone ring labeled D but not shown in Figure 3, was present in the interstage region. It was not used for the results presented here. The diameter of the ANCF duct is 48 in. The radius of the hub is 9 in. at the fan and 12 in. in the aft portion of the duct. Ring C is 5.875 in. forward of the fan centerline, and axial spacings A-B and B-C are 3 in. The spacing of the microphones in the axial arrays is 1.5 in. The forward axial array has a total length of 22.5 in. and the aft axial array is 19.5 in. long. Ring E is located 19 in. aft the fan centerline, or 7.5 in. aft the centerline of the stator ring.

The arrays were combined in different ways for the various types of analysis. Fan imaging made use of the 90-element array resulting from combing the three forward rings: A-B-C. The inlet mode measurements and power estimates used rings A and C together with the forward axial array: A-C-Axial Fwd (76 microphones). Finally, the 44- element array E-Axial Aft was used for the aft mode measurements and power estimates.

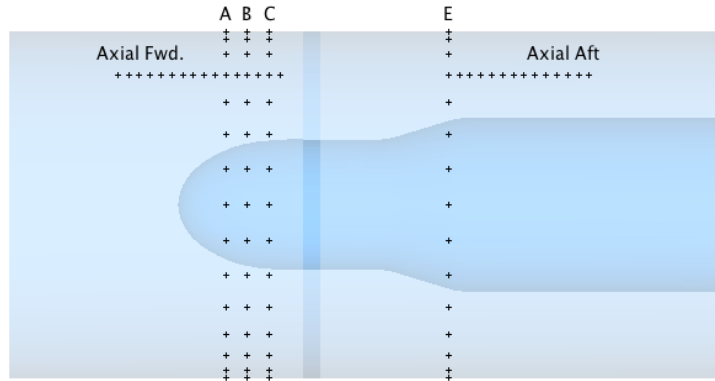


Figure 3.—Microphone array locations in ANCF.

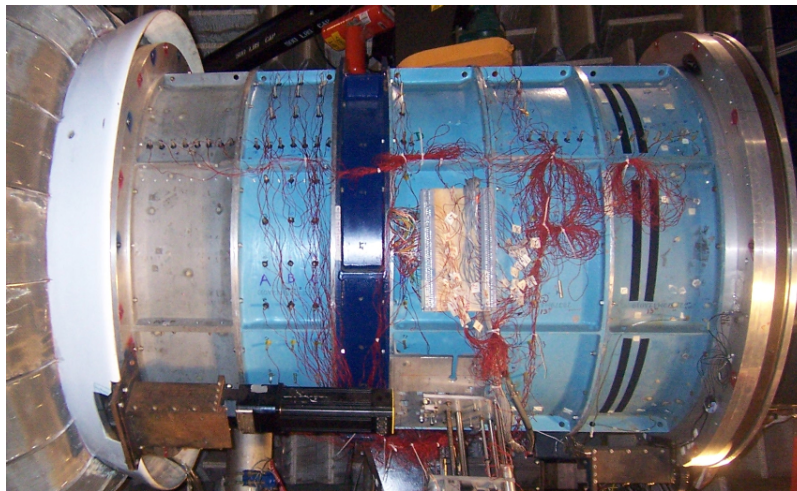


Figure 4.—Microphone installation.

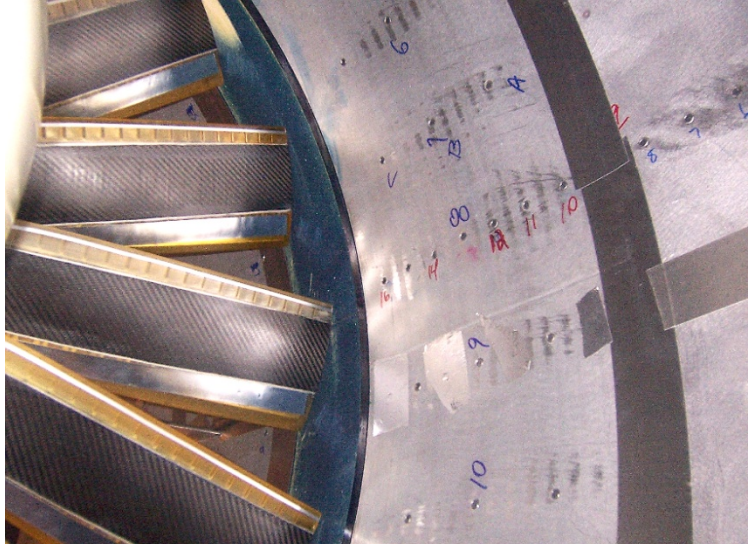


Figure 5.—Inlet microphone arrays.

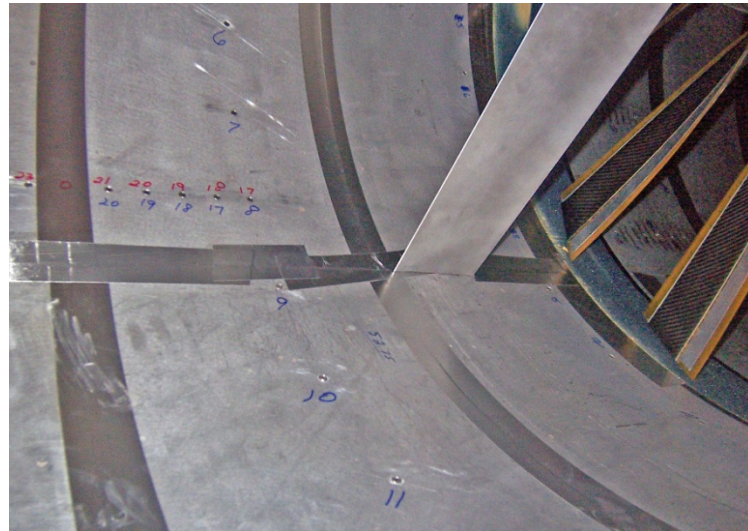


Figure 6.—Aft microphone arrays.

Beamforming Methods

Using Subsets of the CSM Elements

Beamforming in the frequency domain makes use of the array Cross Spectral Matrix (CSM). In wind tunnel beamforming, the diagonal elements of the CSM are usually deleted (Ref. 1) to remove the effect of boundary layer noise from the results. In the current work, it was observed that microphone pairs at the same clock angle showed much higher correlation than pairs corresponding to different angles. It is believed that the cause is convected boundary layer turbulence: two microphones experience nearly the same turbulence if they are aligned streamwise. In order to prevent this effect from contaminating the beamforming results, portions of the CSMs corresponding to streamwise-aligned microphones were set to zero. This modification of the CSM also improved the modal resolution characteristics of the arrays. The patterns used for the mode measurement arrays are shown in Figure 7.

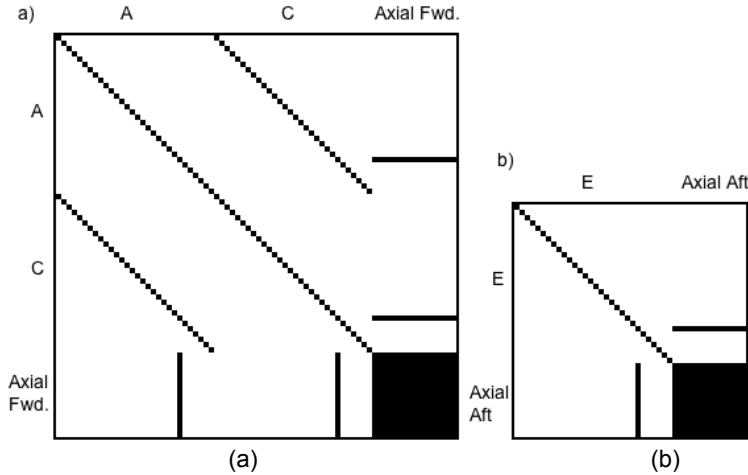


Figure 7.—CSM elements sets S . Elements included are white. (a) A-C-Axial Fwd. array, (b) E-Axial Aft.

A compact treatment of adapting beamforming for deletion of CSM elements is given in References 2 and 3. Following the notation in the references, deleting certain elements of the CSM produces the trimmed CSM, \bar{C} , where the bar indicates that selected elements have been replaced by 0. Let the set of CSM elements that will be included in the beamforming be denoted $S = \{(\mu, \nu)\}$. Consider a particular source or mode with unit power and index k . Let the array response vector (“steering vector”) for this source be denoted \mathbf{g}_k . Given a measured CSM, the classical beamforming expression for estimating the power of this source is

$$b_k = \mathbf{w}'_k \bar{C} \mathbf{w}_k \quad (1)$$

where the weight vector is a normalized version of the steering vector:

$$\mathbf{w} = \frac{\mathbf{g}}{\sqrt{\sum_{(\mu, \nu) \in S} |g_\mu|^2 |g_\nu|^2}} \quad (2)$$

Bessel Steering Vectors

In many applications of beamforming, it is appropriate to compute \mathbf{g} using free space propagation. This is not the best approach for in-duct beamforming at some frequencies because the duct walls alter the sound waves enough to produce confusing results. The current, in-duct, beamforming is based on hardwall annular duct modes with uniform flow (Ref. 3). For modal beamforming, the steering vector is simply a particular duct mode normalized to unit power and evaluated at the microphone locations. For the imaging function, an expression related to the Green’s function is used:

$$g(\bar{\xi}_\nu, \bar{x}_k) = \sum_{mn} \varphi_{mn}^*(\bar{x}_k) \varphi_{mn}(\bar{\xi}_\nu) \quad (3)$$

where $\bar{\xi}$ is a microphone location, \bar{x} is a beamforming map point, and the sum includes the cuton and mildly cutoff annular duct modes with radial order n and spinning order m . As noted in Reference 3 an acoustic pressure normalization of the beamform map is used for the imaging case.

DAMAS Deconvolution

If only a single source is present, the beamform map will typically show that source with a peak level indicating the correct power. However, it will also incorrectly show both nearby sources (beamwidth) and remote sources (sidelobes) with nonzero power. This is described by the array point spread function (PSF), denoted by matrix \mathbf{A} , which can be calculated from

$$A_{jk} = \mathbf{w}_j' \bar{\mathbf{C}}_k \mathbf{w}_j \quad (4)$$

where j is the beamforming point, the source is at k , and the single-source CSM (before trimming) is

$$\mathbf{C}_k = \mathbf{g}_k \mathbf{g}_k' \quad (5)$$

The diagonal elements of \mathbf{A} are unity by construction. The matrix can be very large, and is not necessarily symmetric. Suppose there are mutually incoherent sources at the beamforming points, or modes, and that the source powers are used to make a column vector, \mathbf{X} . Source incoherence means that the CSM can be written

$$\mathbf{C} = \sum \mathbf{C}_k \mathbf{X}_k \quad (6)$$

Using \mathbf{Y} to represent the classical beamform map, the source powers, the PSF, and the beamforming results are related by

$$\mathbf{Y} = \mathbf{A}\mathbf{X} \quad (7)$$

The DAMAS deconvolution algorithm (Ref. 4) consists of beamforming to create \mathbf{Y} and then solving Equation (7) iteratively for \mathbf{X} , subject to the constraint $\mathbf{X}_k \geq 0$. In the current work, like Reference 4, Gauss-Seidel iteration was used, with alternating forward and backward loops over the indices. In some cases, it was found necessary to apply Successive Under Relaxation (SUR) with relaxation parameter $\omega = 0.1$ in order to achieve convergence.

CLEAN-SC Deconvolution

Like DAMAS, CLEAN-SC (Ref. 2) is an algorithm that computes a set of source powers to account for an initial, classical, beamform map. The result, a “clean” map is constructed from the original, “dirty,” map using an iterative procedure. During each iteration, the highest point in the dirty map is identified and a portion of the power at this grid point is transferred to the clean map. A model for the portion of the CSM associated with this partial source is constructed. The model is computed from the (dirty) CSM and the steering vectors in such a way that any sources coherent with the identified peak are included in the model. The last steps in the iteration are to subtract the beamform map of the model CSM from the dirty map and model CSM from the dirty CSM. The iteration is complete when no significant sources remain in the dirty map. Like the DAMAS result, the clean map is intended to represent the true source distribution. One important difference between CLEAN-SC and DAMAS is that multiple coherent sources will probably be represented as a single source in the CLEAN-SC map, with a power matching the highest classical beamform point for the sources. The version of DAMAS used here is not formulated to operate correctly for the coherent case, but it is at least possible that the multiple sources will give rise to distinct peaks in the DAMAS result. Efforts are underway to extend DAMAS to the coherent case (Ref. 5).

Fan Source Imaging

The computation of the fan source images makes use of the microphone rings ahead of the fan, array A-B-C. Tone noise is removed and the broadband data set is resampled to a coordinate system that rotates with the fan. As discussed in Reference 3, each 30-microphone, real, subarray is replaced with a 32-element ring of virtual microphones. The coordinates of the virtual microphones are fixed relative to the fan blades. Beamforming is then performed as if the array were a conventional, fixed, phased array. The only modification to the process needed for the rotation is to account for the apparent swirl in the rotating coordinate system in determining the set of cuton annular duct modes and their axial propagation constants when evaluating Equation (3). DAMAS or CLEAN-SC deconvolution is sometimes applied to produce the final results.

As presented in Reference 3, the annular duct modes in the rotating coordinate system are characterized by an effective wave number

$$k_{0\text{eff}} = k_0 - \frac{m'\Omega}{c} \quad (8)$$

where $k_0 = \frac{\omega}{c}$, m' is the spinning order in the rotating coordinate system (which is the same as m , the spinning order in the stationary system), and Ω is the fan rotation frequency. Multiplying by the speed of sound, Equation (8) becomes

$$\omega_{\text{eff}} = \omega - m\Omega \quad (9)$$

The spinning order and effective wave number $k_{0\text{eff}}$ are used to determine the radial eigenvalues and the axial propagation constants. In this work, the values of m are limited by the spacing of the virtual microphones to $-16 < m < 16$. Using the corrected speed as an approximation, Ω is 188.5 radians/sec. The largest value of $m\Omega$ is therefore 2827 radians/sec. or 450 Hz. Potential difficulties with a negative effective wavenumber were avoided by limiting the analysis to frequencies above 450 Hz. In higher-speed applications, it has been found useful to constrain the spinning orders included in the steering vector calculation to $m\Omega < \omega/2$.

Simulation Example

The theoretical resolution of the VRM array with several beamforming techniques is shown in Figures 8 and 9. A mathematical point source was positioned in the fan plane, close to the outer wall, and the steering vector for this source and a synthetic CSM were computed according to Equations (3) and (5). The circumferential location of the source was near the trailing edge of blade 15. The numbering of the blades is such that blades with successively increasing numbers pass a given point in the duct. The trailing edge of blade 15 is therefore the edge near blade 16. The fan rotation speed used in computing the steering vector was 1780 rpm. Using the synthetic CSM in classical beamforming gives the results in Figure 8(a) to (c). There are high sidelobe levels, the radial resolution is poor, and apparent sources exist outside the duct. Using the annular duct steering vectors gives the results in Figures 8(d) to (f). The sidelobes are improved and the map is confined to the duct (by construction). The peak is slightly rotated, to the correct angle, because apparent swirl is taken into account. The radial resolution is still poor. Applying DAMAS gives the results in Figure 9. The resolution is much sharper. A maximum filter with a radius of 2 pixels was applied to Figure 9 and all of the other DAMAS and CLEAN-SC plots in order to show isolated point sources more clearly. There is still evidence of sidelobes in Figure 9(c) and (b). This is believed to be caused by the fact that a trimmed CSM was used in the beamforming, but not in the computation of the PSF for DAMAS in this case. This can be regarded as an illustration of the sensitivity of DAMAS to the accuracy of the PSF.

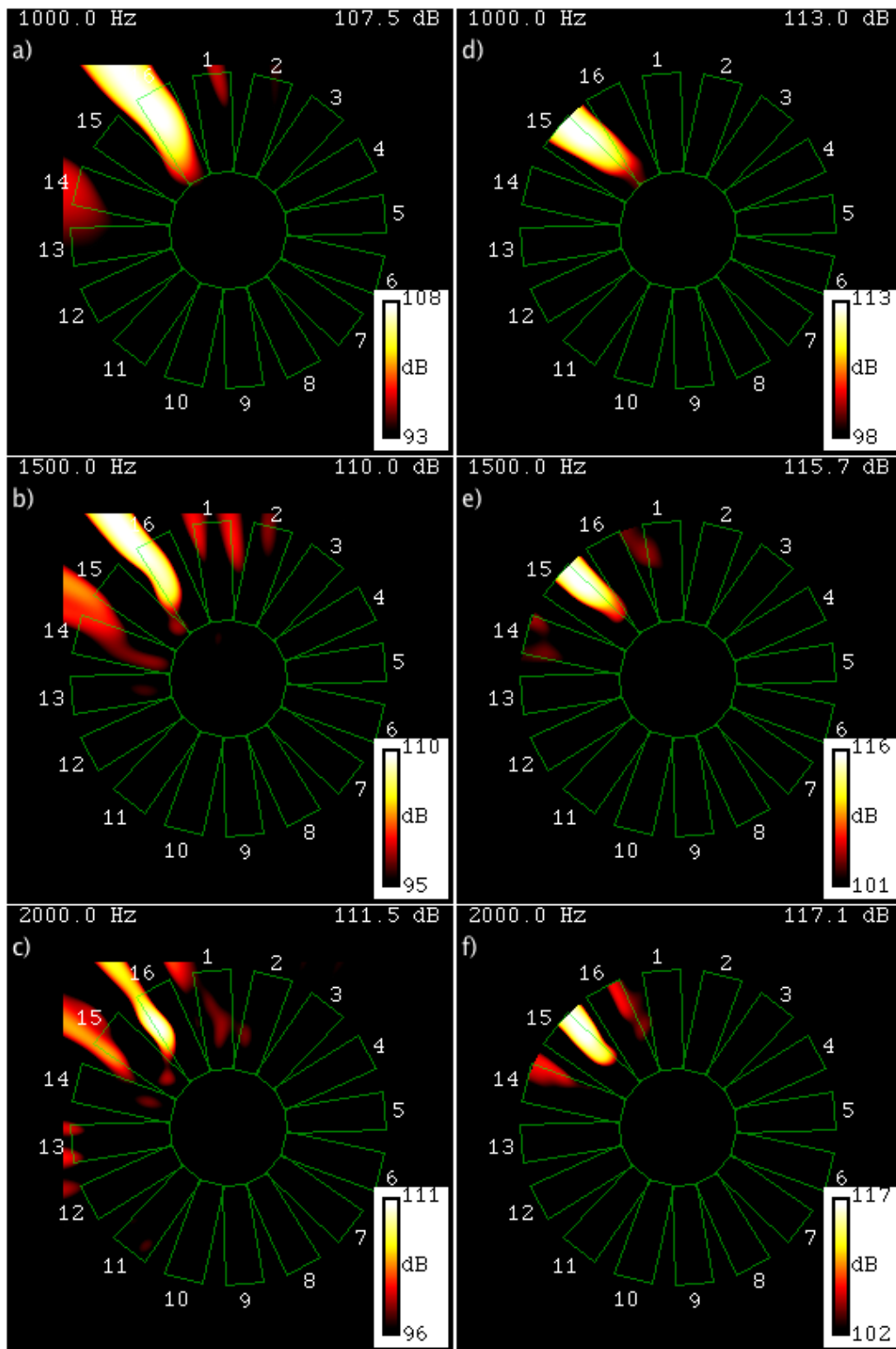


Figure 8.—Beamforming a simulated source. Free space steering vectors, (a) to (c); annular duct mode steering vectors, (e) to (f).

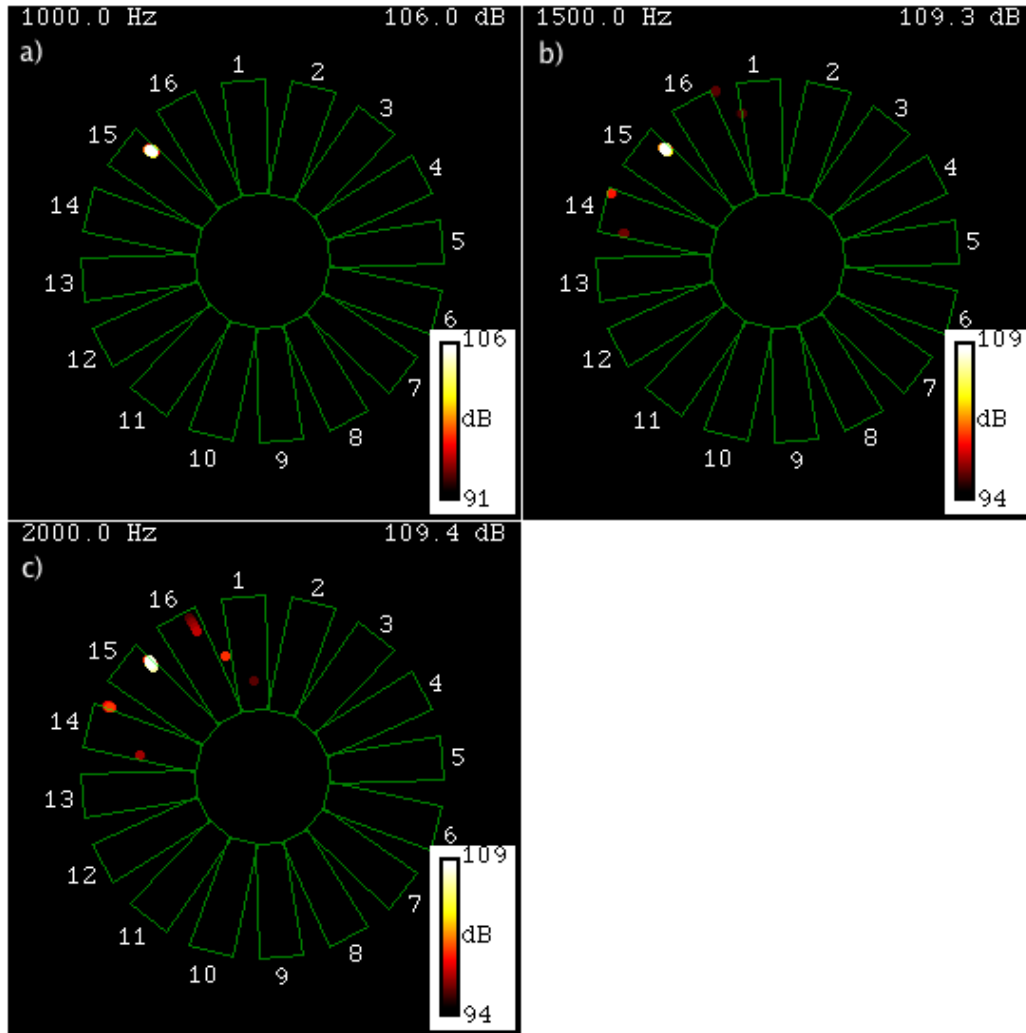


Figure 9.—Beamforming a simulated source: DAMAS. Maximum filter with a radius of 2 pixels applied to make small spots visible.

Mode and Power Measurements

Mode maps and power estimates are made using data from the inlet array A-C-Axial Fwd and the aft array E-Axial Aft. Tone removal is performed and the broadband microphone signals are used to compute CSMs. Outward-propagating cuton modes are considered for each frequency. The steering vector for mode (m,n) (spinning order, radial order) and microphone location $\vec{\xi}_v$ is

$$g(\vec{\xi}_v, (m, n)) = \frac{1}{P_{mn}} \phi_{mn}(\vec{\xi}_v) \quad (10)$$

where P_{mn} is the power of the mode that was initially normalized to unity average-square pressure over a cross section of the duct. Beamforming with Equation (1) using these steering vectors produces the mode map. A power estimate is obtained by summing the powers of the determined modes. Since the arrays do not have perfect modal resolution, it is not strictly appropriate to sum the powers of modes in the raw beamform map; this would be expected give a result that is too high. Deconvolution should be applied first. The modes may be mutually coherent or incoherent. (To see that it is possible to have coherent modes, suppose hypothetically that all of the sound is created by a single point source. Since all of the

modes have the same origin, they must be temporally coherent.) Inspection of the power integral and application of the mutual orthogonality of the modes shows that mode powers should be summed whether the modes are coherent or incoherent. The available deconvolution techniques include DAMAS and CLEAN-SC. DAMAS is not strictly appropriate if the modes are coherent, but the powers in the resulting deconvolved maps are the appropriate quantities to sum. CLEAN-SC may apply in the coherent case, but does not account for coherent mode powers appropriately to support the final power estimate.

Simulation Example

Figure 10 gives beamforming results for a simulated (7,1) mode with a power of 100 dB re. 1 pW. Figures 10(a) to (c) represent the inlet and Figures 10(d) to (e) are simulations of the aft duct. The cuton modes at the analysis frequency of 1503 Hz are shown in blue. The aft duct has fewer cuton radial modes because of its smaller duct height (12 in. vs. 15 in. forward of the fan) and the direction of the flow, assumed to be Mach 0.1. The classical beamforming plots show that both arrays have excellent resolution in m (as they should, since they contain complete rings), but poor resolution in the n . The correct power, 100 dB re. 1 pW, was determined for the true mode, but the total power for the classical beamforming overestimates the true value as a result of including the radial-order sidelobes. As an aside, deleting the axial-axial portion of the CSM is critical to the good m -order resolution of these arrays. If the full CSMs are included, apart from the diagonals, of course, the resolution in spinning order becomes poor. This is similar to cross array beamforming (Ref. 6).

Applying DAMAS or CLEAN-SC (Figs. 10(b), (c), (e), and (f)) removes the radial order peak spreading and restores the correct total power, although CLEAN-SC loses 0.08 dB in this case.

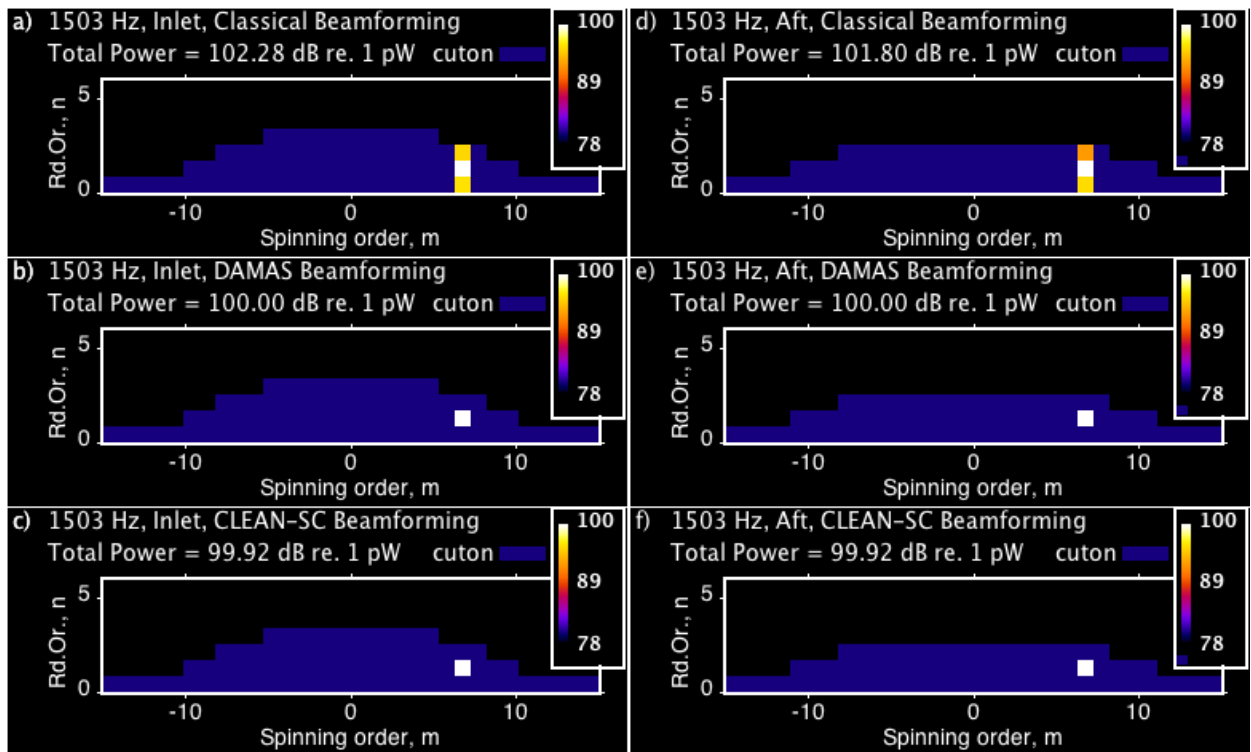


Figure 10.—Mode plots for a simulated source. Inlet, (a) to (c); aft, (d) to (f).

Data and Configurations

Results are given for 1800 rpm (corrected) and five configurations. The baseline configuration, A-I has 16 nominally identical blades. The blades used for the test were old and had a number of nonuniformities such as chipped corners and loose pieces of tape (Fig. 11(b) to (d)). The second configuration for the results, A-II had blades #6 and #14 replaced with alternate blades with missing trailing edges (Fig. 11(a)). In configuration A-III, two plastic bolts were installed in each of blades #6 and #14 to create flow noise at part-span locations (Fig. 11(e)). Configuration A-VII was similar to configuration A-III, except the bolts were removed, leaving two holes in blade #6 and two holes in blade #14. In configuration, A-VIII, blades #6 and #14 were removed entirely. The data for blade imaging (Array A-B-C) were acquired synchronously at 600 samples per revolution for a nominal sampling rate of 18,000 Hz. The data for mode and power measurement (arrays A-C-Axial Fwd and E-Axial Aft) were acquired asynchronously at 20,000 Hz. The analysis makes use of 20 sec of data from each condition.

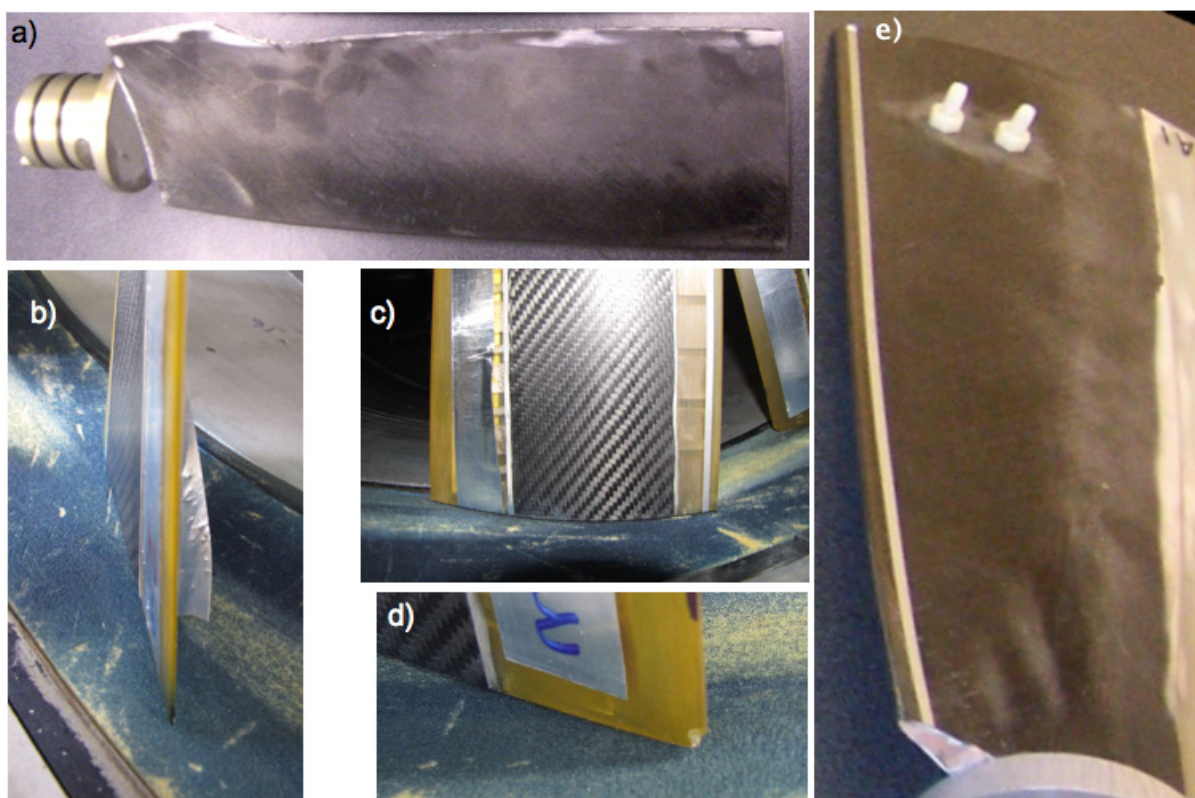


Figure 11.—Blade details. Removed trailing edge, (a), loose tape, (b) and (c), chipped corner, (d), added bolts, (e).

Results

Imaging Results

VRM imaging plots for the baseline configuration at three frequencies using two sets of beamforming steering vectors are shown in Figure 12. As in Figure 8, parts (a) to (c) give results at approximately 1000, 1500, and 2000 Hz using free space steering vectors, and parts (d) to (f) represent steering vectors derived from annular duct modes. Individual blade images can be seen clearly using both sets of steering vectors, but only the annular duct results show the blades at the higher and lower frequencies as well. The annular duct results indicate that the primary source region is the trailing edge of the blades. (The direction of fan rotation is counterclockwise in all of the imaging figures.) The plots using the free space steering vectors show incorrect circumferential source locations because of the effect of apparent swirl. The radial distribution of the apparent source is unclear at the highest frequency.

VRM and VRM/CLEAN-SC results are given for configuration A-II in Figure 13. The part of the blade modification that creates the most noise appears to be the near the hub. As shown in Figure 11(a), the carved blades have sharp corners in the trailing edges near the hub. Figure 13(d) shows bright spots on the modified blades at approximately the radius of the corners, but the spots seem to be closer to the leading edges of the blades than the trailing edges. The direction of the offset is consistent with the inflow swirl created by the fan, i.e., the spots are displaced counterclockwise from the probable source locations. The analysis assumes that the flow is axial in the nacelle coordinate system. (This swirl is physical and is distinct from the apparent swirl of the axial flow in the rotating coordinate system that was taken into account in the mode-based beamforming.) Sources near the blade tips, such as spots at the outer wall in Figure 13(d) are not expected to be strongly influenced by inflow swirl because the propagation distance through the flow to the nearest virtual rotating microphone is relatively short.

Figure 14 shows one frequency from Configuration A-VIII: blades #6 and #14 removed. As expected, the spots at the blade tip trailing edges are missing. It also appears that the main source locations for the following blades, #7, #8, #15, and #16 are displaced away from the wall, presumably as a result of the altered aerodynamic environment seen by these blades.

The configuration with plastic bolts in blades #6 and #14, A-III, is treated in Figure 15. The strongest source at the lower frequencies is on blade #2. Sources like this appeared when pieces of tape pulled loose from the fan, as shown in Figure 11(b). The bolts are represented by spots on blades #7 and #15 at 1096 and 1164 Hz, and blades #6 and #14 at 3972 Hz. Viewed in the fan coordinate system, the bolt source location appears farther downstream at lower frequency. This phenomenon is familiar in, for example, flap edge noise (Ref. 7) and jet mixing noise (Ref. 8). At the lowest frequency shown in Figure 15, the bolt source appears at the outer wall and extends from the blade with the bolt to the following blade. This may be caused by interaction between the wakes of the bolts and the blade tip vortices. At 4451 Hz, sources appear near the roots of the leading edges of blades #6 and #14. These appear similar to the case of the missing trailing edge (Fig. 13(d)). The trailing edges of blades #6 and #14 in Configuration A-III were present, but featured a different design from the other blades. These, nonuniform, trailing edges may act as noise sources similar to Configuration A-II.

Plots from Configuration A-VII, bolt holes in blades #6 and #14, are shown in Figure 16. The low frequency spot on blade #2 is missing because the tape on this blade was repaired between the runs for Configurations A-III and A-VII. Spots near the leading edge of the tip of blades #7 and #15 are apparent at 935 Hz, but the sources are more compact and lower in level than the case with the bolts installed (69 dB vs. about 74 dB at 890 Hz in Fig. 15). The plot for 1136 Hz in Figure 16 shows the blade tip trailing edges more clearly than the corresponding plot for the bolts, 1164 Hz in Figure 15, which is dominated by the source on blade #2 and the bolt noise that appears on blades #7 and #14. Bolt hole noise is evident at 3808 and 4008 Hz. The high frequency noise seen at the leading edges of blades #6 and #14 in Figure 15 is not evident in Figure 16. This may be a result of masking by a new source that appeared on blade #3.

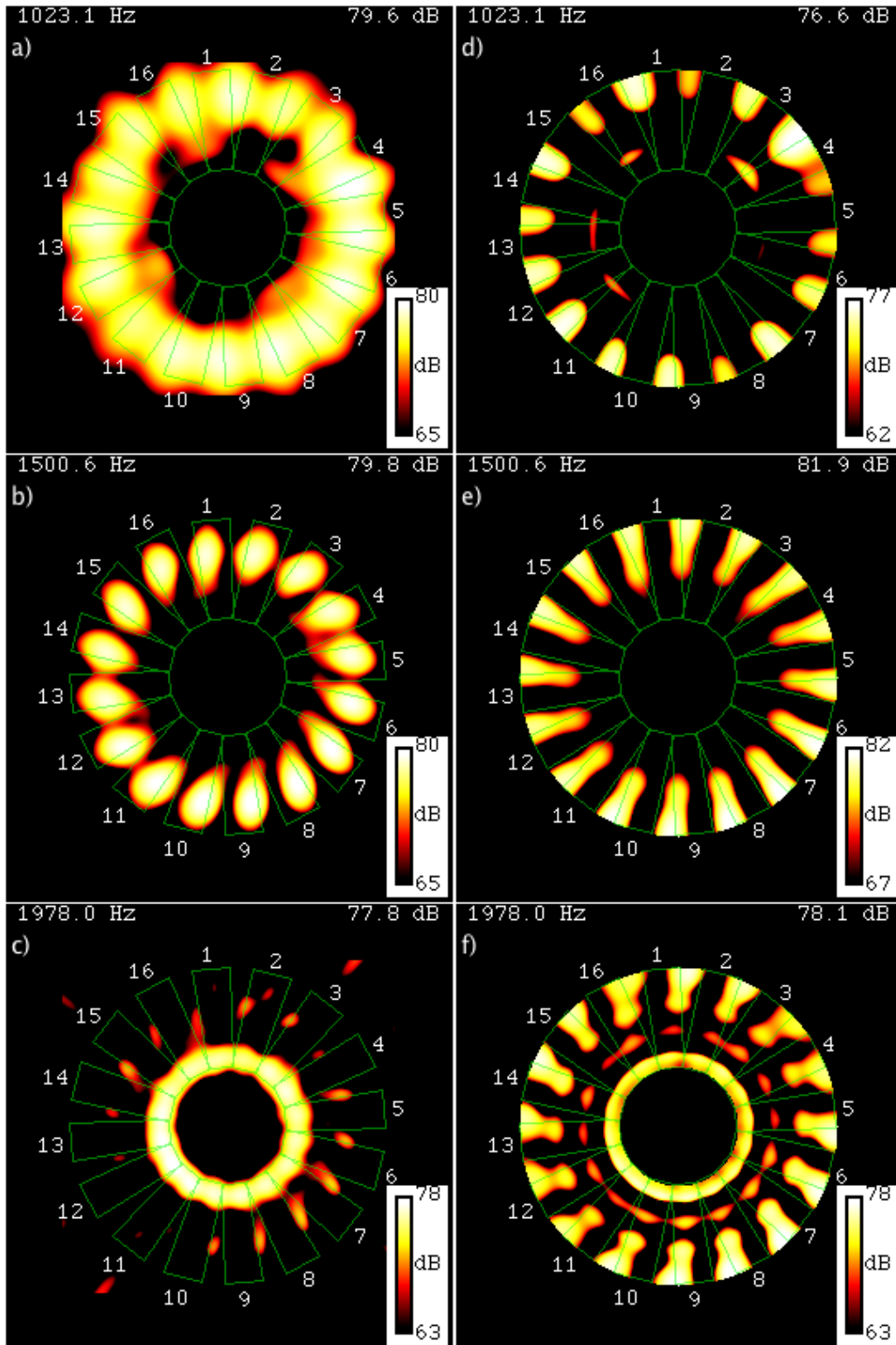


Figure 12.—Beamforming the baseline configuration. Free space steering vectors, (a) to (c); annular duct mode steering vectors, (d) to (f).

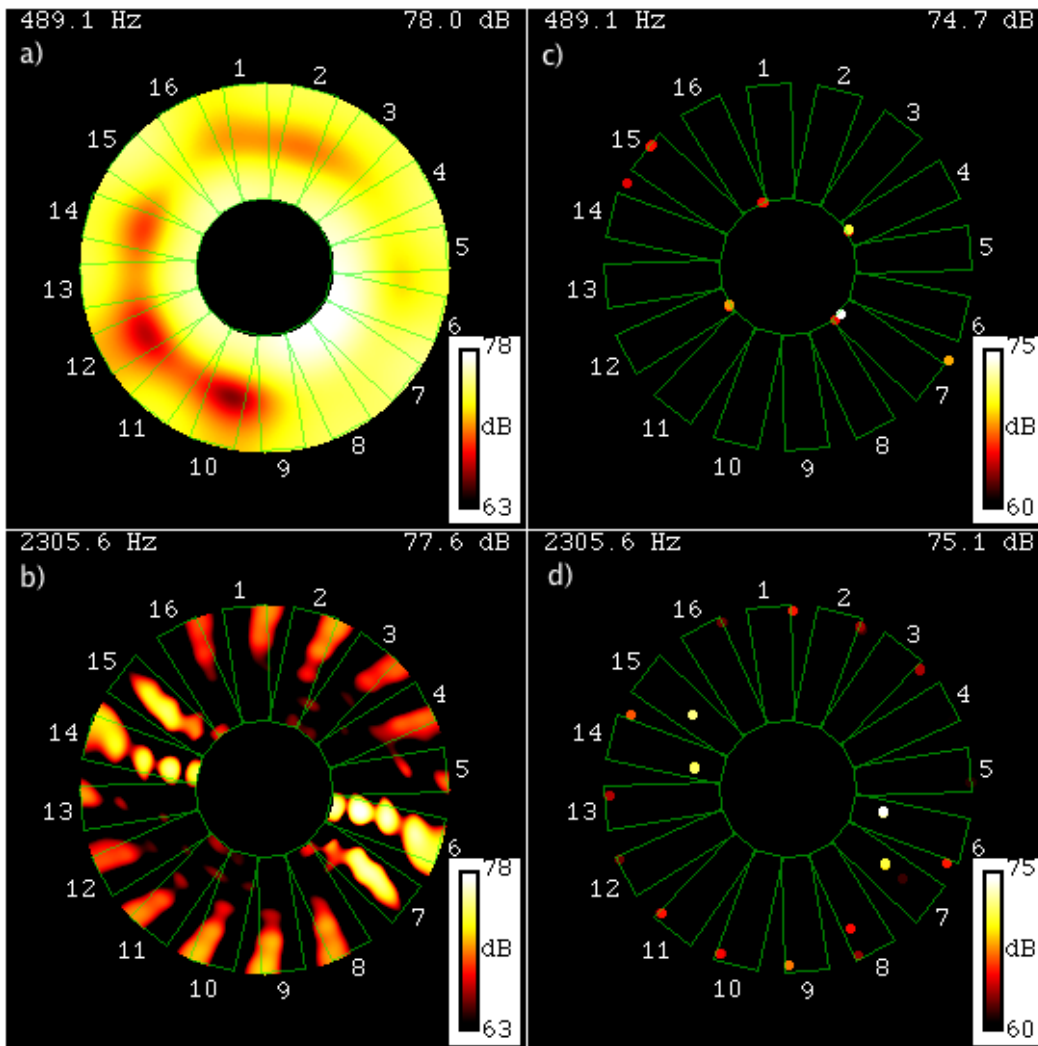


Figure 13.—Configuration A-II (TE missing on blades #6 and #14). VRM, (a) and (b); VRM/CLEAN-SC, (c) and (d).

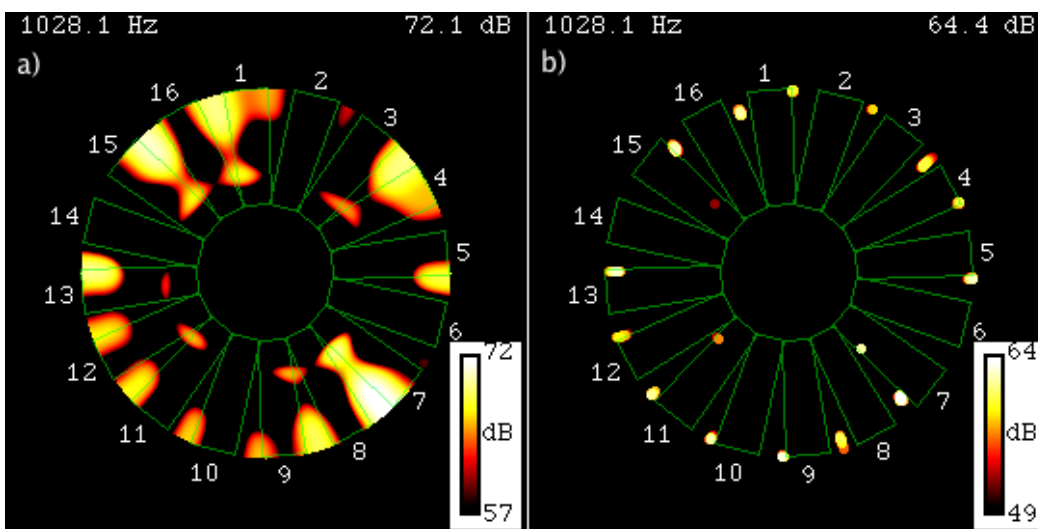


Figure 14.—Beamforming for Configuration A-VIII. Blades #6 and 14 removed, VRM. (a); VRM/DAMAS, (b).

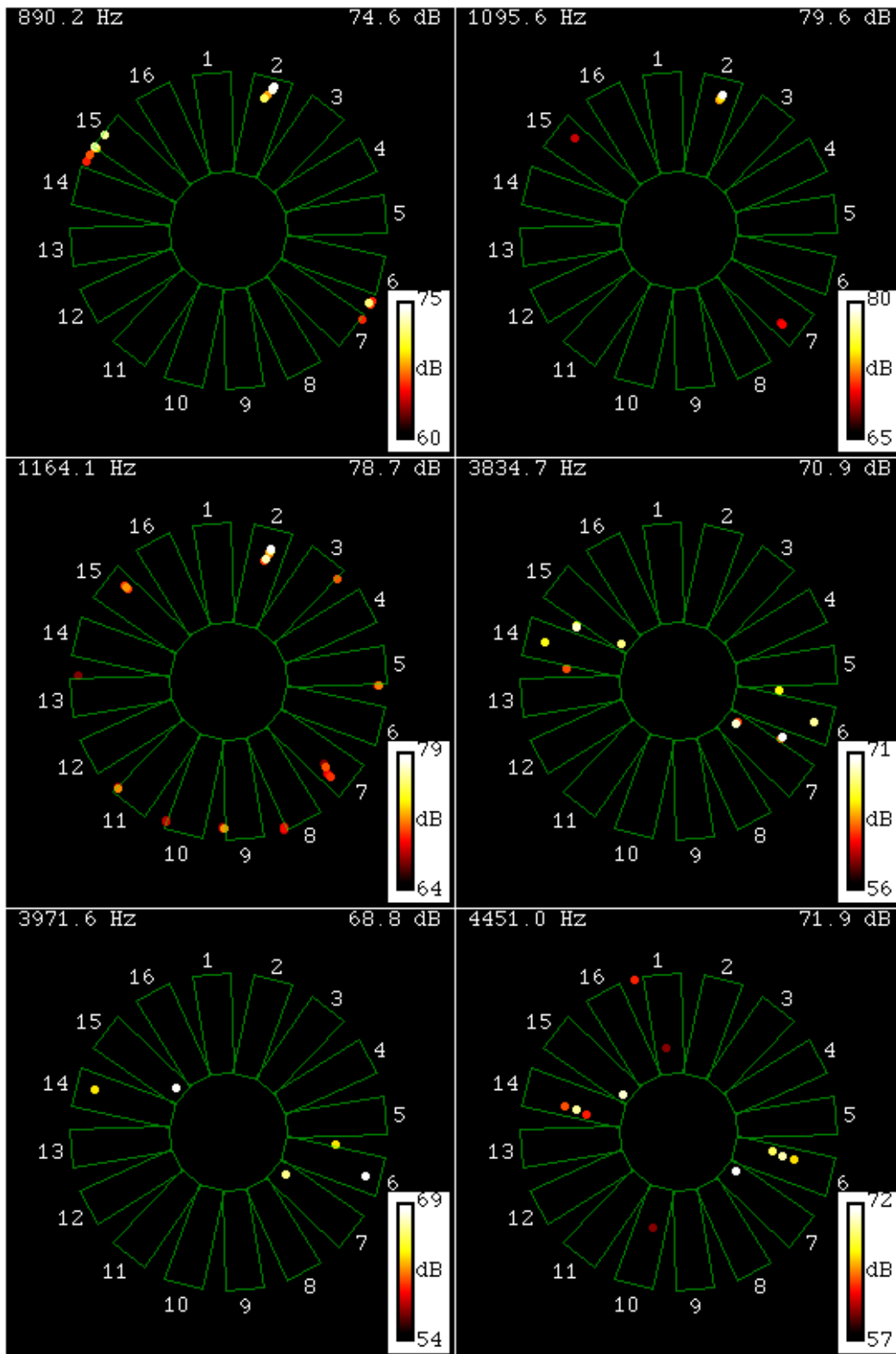


Figure 15.—VRM/CLEAN-SC beamforming for configuration A-III. Bolts in blades #6 and #14.

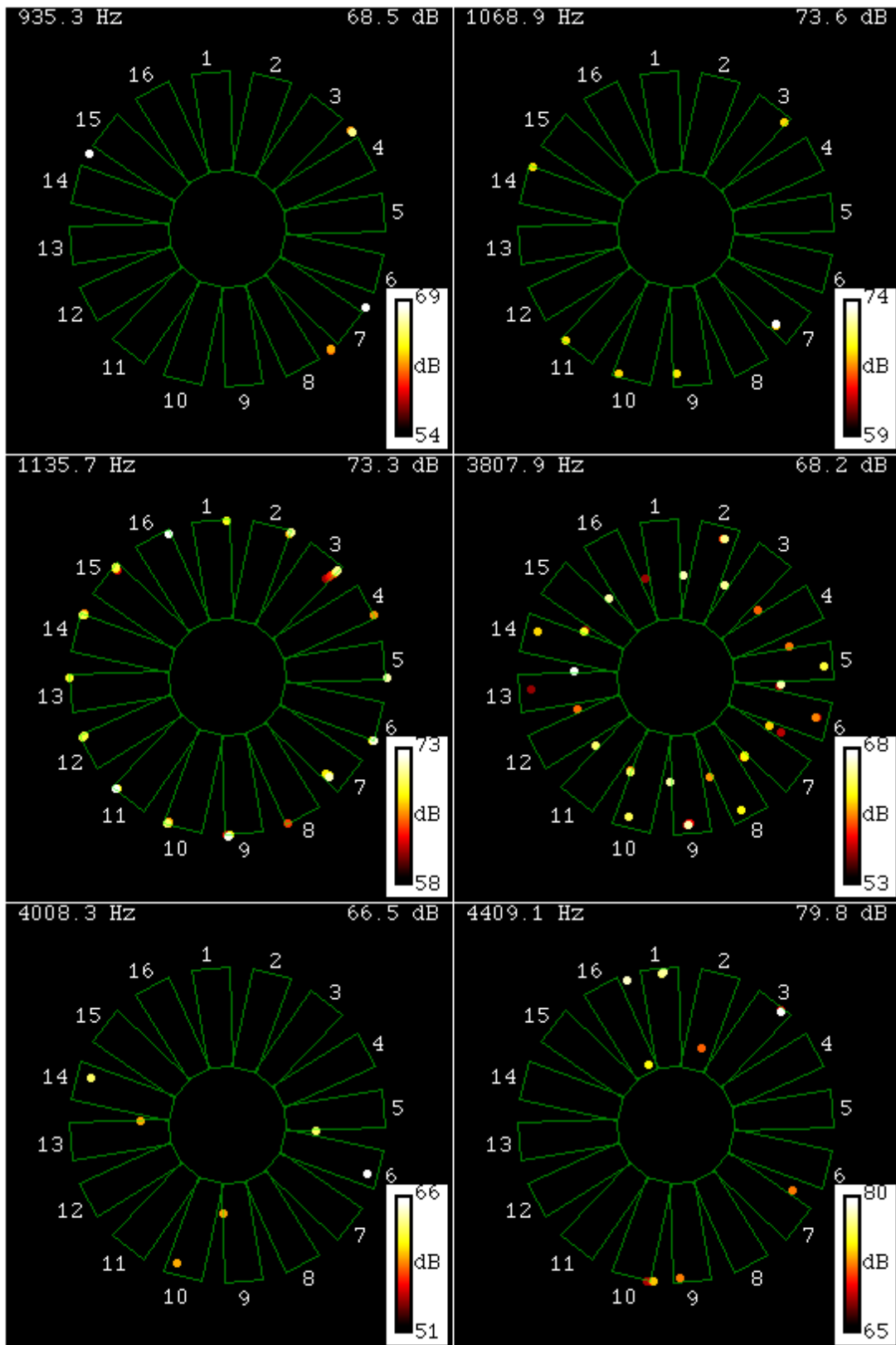


Figure 16.—VRM/CLEAN-SC beamforming for configuration A-VII. Bolt holes in blades #6 and #14.

Modes

Mode plots for Configuration A-I at 1503 Hz are given in Figure 17. Parts (a) to (c) present modes in the inlet and (d) and (e) represent the fan duct. In each case, three types of beamforming are shown: classical, DAMAS, and CLEAN-SC. The plots also note the estimate for the total power obtained by summing the mode powers for this 9.76 Hz (20,000 Hz/2048) frequency bin. The DAMAS results show reduced levels for some of the modes such as $(m,n) = (-5,1)$ in the inlet and $(4,1)$ in the fan duct that represent imperfect radial order resolution in classical beamforming. The power results for DAMAS are consequently lower than the classical values by 1.77 dB in the inlet and 1.35 dB in the fan duct.

The CLEAN-SC plots, Figures 17(c) and (f), show significantly fewer modes than the classical or the DAMAS plots. The interpretation is that modes present in the baseline plots but missing from the CLEAN-SC plots were coherent with other modes that are shown in the CLEAN-SC plots. The power of these missing modes is also missing from the total power results, which are consequently much lower than the classical values (by 4.02 dB for the inlet and 5.33 dB for the aft case).

Total Power

The inlet and aft power levels for three frequency bands are shown in Figure 18. The bands are 1: 237-711, 2: 711-1186, and 3: 1186-1659 Hz. These bands are centered at the nominal blade passage frequency and its second and third harmonics. The bars in Figure 18 correspond to the integrated power levels from the far field microphones (blue), the mode results from classical beamforming (red), and the DAMAS mode results (yellow). The rms errors, taken as the differences between the far field and the modal results over all three configurations, inlet and aft, and the three frequency bands (18 data points) are 1.05 dB for classical beamforming and 1.907 dB for DAMAS.

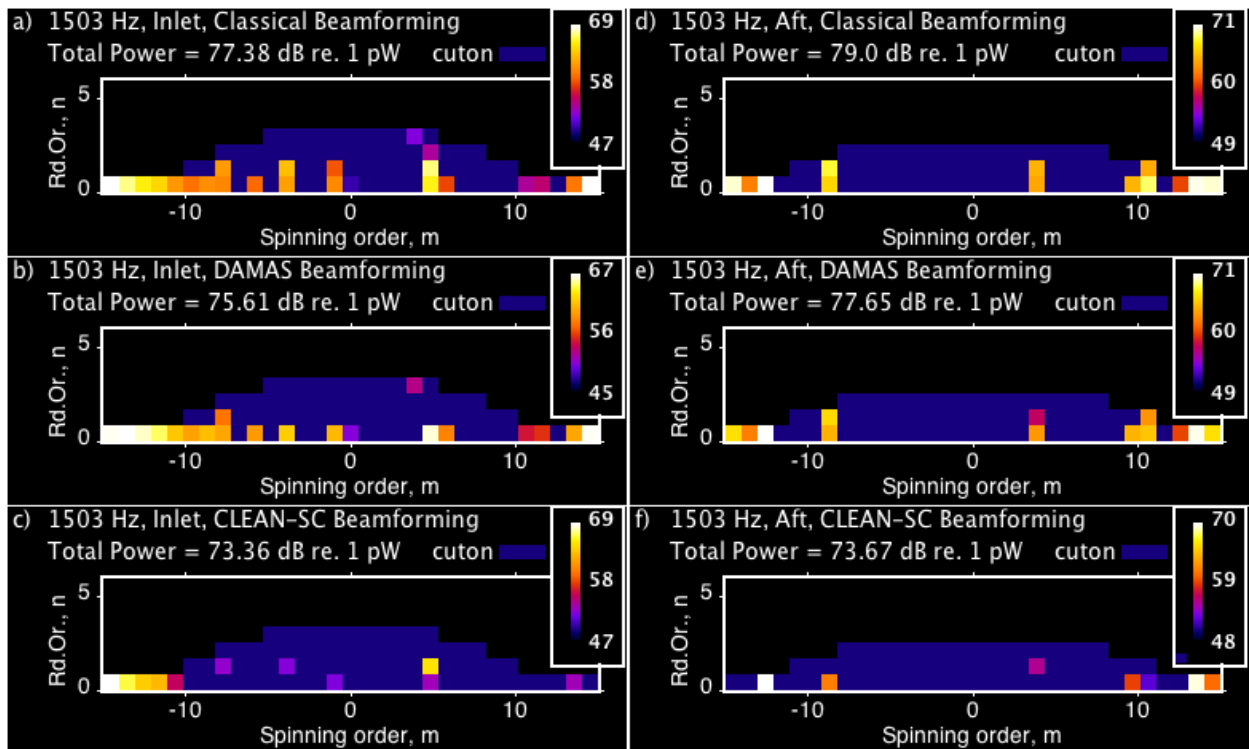


Figure 17.—Mode plots for the baseline configuration. Inlet, (a) to (c); aft, (d) to (f).

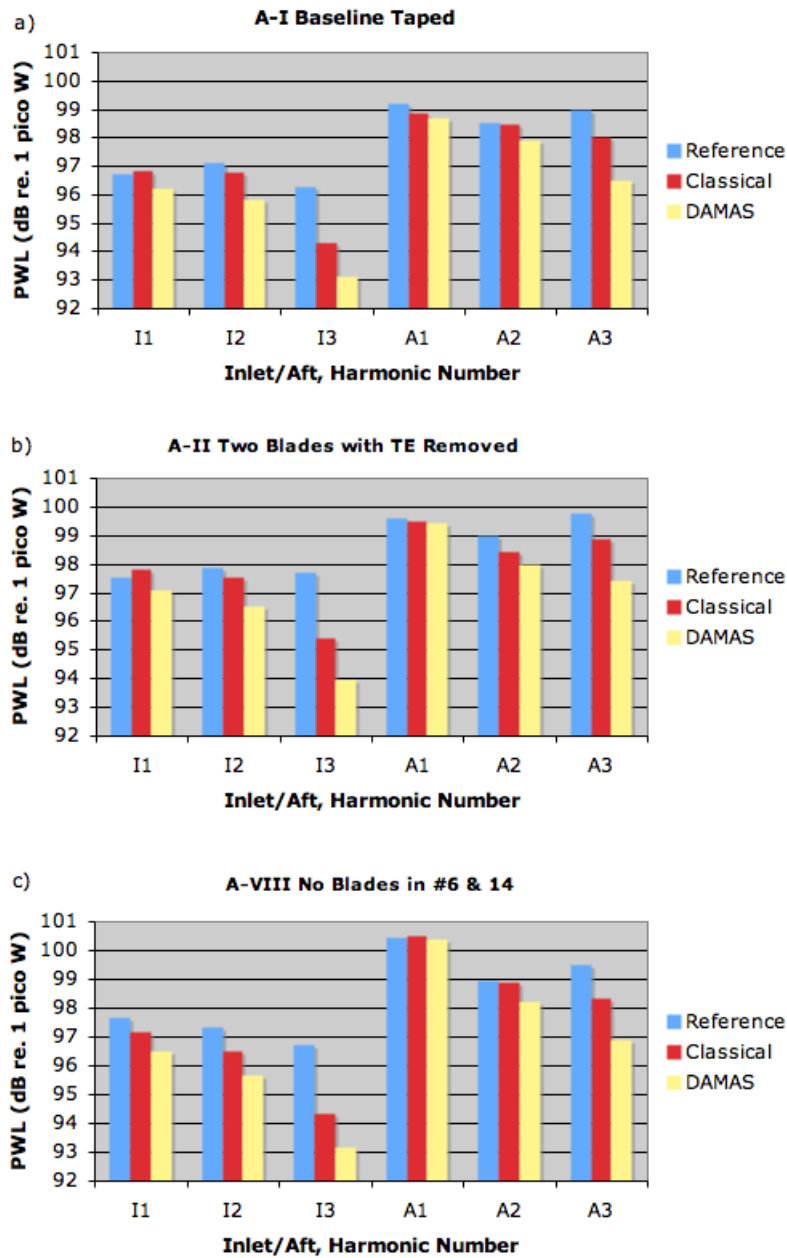


Figure 18.—Power results for the inlet (I) and the Aft duct (A) for three frequency bands: 1: 237-711 Hz, 2: 711-1186 Hz, and 3: 1186-1659 Hz. Far field reference values and modal results using classical beamforming and DAMAS.

Analysis of the *Power Results*

The classical power results appear to be more accurate than the DAMAS results, but this may represent cancellation of two sources of error: extra power from imperfect resolution of radial modes, as discussed previously (increases power values) and decorrelation of the CSM elements by propagation through boundary layer turbulence (Ref. 9), which decreases the power results. Both error sources increase with frequency. The modal resolution effect becomes more important at higher frequency because there are more radial modes cut on, and the decorrelation becomes more important because the propagation time shifts are a larger portion of an acoustic period. The DAMAS results contain only the decorrelation error, so they are lower than the far field values, and the difference is greater at higher frequency.

Conclusions

Virtual rotating microphone arrays can be used to image broadband fan source distributions. Steering vectors computed from annular duct modes and the DAMAS and CLEAN-SC deconvolution increase the frequency range of applicability and the resolution of the method. The VRM/deconvolution images showed noise from blade tip trailing edges, bolts installed in blades, pieces of loose tape, and nonuniformities near the root of blade trailing edges. Circumferential and radial resolution were demonstrated.

In-duct arrays combining rings and axial line arrays are effective for broadband mode measurements and sound power calculations. It is appropriate to delete the portion of the CSM representing the cross powers of microphones within the line array. In-duct power estimates obtained from the classical beamforming mode measurements agree with the far field sound power measurements to within about 1 dB.

References

1. Dougherty, R.P., "Beamforming in acoustic testing," Chapter 2 in *Aeroacoustic Testing*, T.J. Mueller, ed., Springer-Verlag, 2002.
2. Sijtsma, P., "CLEAN Based on Spatial Source Coherence," AIAA Paper 2007-3436, May, 2007.
3. Dougherty, R.P. and B.E. Walker, "Virtual rotating microphone imaging of broadband fan noise," AIAA Paper 2009-3121, May 2009.
4. Brooks, T., and W. Humphreys, "A Deconvolution Approach for the Mapping of Acoustic Sources (DAMAS) Determined from Phased Microphone Arrays," AIAA Paper 2004-2954, May, 2004.
5. Brooks, T., and W. Humphreys, "Extension of DAMAS phased array processing for spatial coherence determination (DAMAS-C)," AIAA Paper 2006-2654, May 2006.
6. Piet, J.-F., and J. Elias, "Airframe Noise Source Localization Using a Microphone Array," AIAA Paper 97-1643, Atlanta, GA, May 12–14, 1997.
7. Kendall, J.M. and W.F. Ahtye, "Noise Generation by a Lifting Wing/Flap Combination at Reynolds Numbers to 2.8×10^6 ," AIAA Paper 80-0035, Jan. 1980.
8. Dougherty, R.P. and G.G. Podboy, "Improved Phased Array Imaging of a Model Jet," AIAA Paper 2009-3186, May 2009.
9. Dougherty, R.P., "Turbulent decorrelation of aeroacoustic phased arrays: lessons from atmospheric science and astronomy," AIAA Paper 2003-3200, May 2003.

REPORT DOCUMENTATION PAGE			Form Approved OMB No. 0704-0188		
<p>The public reporting burden for this collection of information is estimated to average 1 hour per response, including the time for reviewing instructions, searching existing data sources, gathering and maintaining the data needed, and completing and reviewing the collection of information. Send comments regarding this burden estimate or any other aspect of this collection of information, including suggestions for reducing this burden, to Department of Defense, Washington Headquarters Services, Directorate for Information Operations and Reports (0704-0188), 1215 Jefferson Davis Highway, Suite 1204, Arlington, VA 22202-4302. Respondents should be aware that notwithstanding any other provision of law, no person shall be subject to any penalty for failing to comply with a collection of information if it does not display a currently valid OMB control number.</p> <p>PLEASE DO NOT RETURN YOUR FORM TO THE ABOVE ADDRESS.</p>					
1. REPORT DATE (DD-MM-YYYY) 01-12-2010		2. REPORT TYPE Technical Memorandum		3. DATES COVERED (From - To)	
4. TITLE AND SUBTITLE Locating and Quantifying Broadband Fan Sources Using In-Duct Microphones			5a. CONTRACT NUMBER NNC07CB02C		
			5b. GRANT NUMBER		
			5c. PROGRAM ELEMENT NUMBER		
6. AUTHOR(S) Dougherty, Robert, P.; Walker, Bruce, E.; Sutliff, Daniel, L.			5d. PROJECT NUMBER		
			5e. TASK NUMBER		
			5f. WORK UNIT NUMBER WBS 561581.02.08.03.18.03		
7. PERFORMING ORGANIZATION NAME(S) AND ADDRESS(ES) National Aeronautics and Space Administration John H. Glenn Research Center at Lewis Field Cleveland, Ohio 44135-3191			8. PERFORMING ORGANIZATION REPORT NUMBER E-17508		
9. SPONSORING/MONITORING AGENCY NAME(S) AND ADDRESS(ES) National Aeronautics and Space Administration Washington, DC 20546-0001			10. SPONSORING/MONITOR'S ACRONYM(S) NASA		
			11. SPONSORING/MONITORING REPORT NUMBER NASA/TM-2010-216931		
12. DISTRIBUTION/AVAILABILITY STATEMENT Unclassified-Unlimited Subject Category: 71 Available electronically at http://gltrs.grc.nasa.gov This publication is available from the NASA Center for AeroSpace Information, 443-757-5802					
13. SUPPLEMENTARY NOTES					
14. ABSTRACT In-duct beamforming techniques have been developed for locating broadband noise sources on a low-speed fan and quantifying the acoustic power in the inlet and aft fan ducts. The NASA Glenn Research Center's Advanced Noise Control Fan was used as a test bed. Several of the blades were modified to provide a broadband source to evaluate the efficacy of the in-duct beamforming technique. Phased arrays consisting of rings and line arrays of microphones were employed. For the imaging, the data were mathematically resampled in the frame of reference of the rotating fan. For both the imaging and power measurement steps, array steering vectors were computed using annular duct modal expansions, selected subsets of the cross spectral matrix elements were used, and the DAMAS and CLEAN-SC deconvolution algorithms were applied.					
15. SUBJECT TERMS Fan noise; Phased array					
16. SECURITY CLASSIFICATION OF:			17. LIMITATION OF ABSTRACT UU	18. NUMBER OF PAGES 25	19a. NAME OF RESPONSIBLE PERSON STI Help Desk (email:help@sti.nasa.gov)
a. REPORT U	b. ABSTRACT U	c. THIS PAGE U			19b. TELEPHONE NUMBER (include area code) 443-757-5802

